Research Square

Preprints are preliminary reports that have not undergone peer review.
They should not be considered conclusive, used to inform clinical practice,
or referenced by the media as validated information.

Targeting oxidative phosphorylation to impair tumor-initiating properties of triple- negative breast cancer stem-like cells

Cemile Uslu
Sabanci University
Esra Akkuş
Sabanci University
Mert Güngör
Sabanci University
Eda Kapan
University Pompeu Fabra (UPF)
Can Tunçay
University Pompeu Fabra (UPF)
Zeynep Ulker
King's College London
Alex Lyakhovich
alex.lyakhovich@sabanciuniv.edu

Sabanci University

Research Article

Keywords:

Posted Date: November 17th, 2026

DOI: https://doi.org/10.21203/rs.3.rs-11472784/v1

License: This work is licensed under a Creative Commons Attribution 4.0 International License.
Read Full License

Additional Declarations: No competing interests reported.

Abstract

Cancer stem-like cells (CSCs) have been implicated in tumor recurrence, therapeutic resistance, and metastatic progression, making their metabolic dependencies potential therapeutic targets. We investigated oxidative phosphorylation (OXPHOS) as a metabolic vulnerability of triple-negative breast cancer (TNBC) stem-like cells and evaluated the effects of mitochondrial metabolic intervention in vitro and in vivo. Mammosphere-derived cells exhibited enhanced mitochondrial respiration. Building on our previous findings that the repurposed antimicrobials amoxicillin (AMX) and fosmidomycin sodium salt (FSS) inhibit OXPHOS, we now demonstrate that these agents also suppress mammosphere formation, reduce mitochondrial respiratory activity, and increase oxidative stress and mitophagy in CSC-like TNBC cells. In vivo, mammosphere-derived cells exhibited increased metastatic potential, as indicated by greater lymph-node enlargement and lung nodule burden, which were significantly reduced by AMX treatment. In a complementary tumor-establishment model, administration of AMX for approximately two weeks before cell implantation delayed subsequent tumor development. These findings indicate that targeting mitochondrial metabolism can impair tumor establishment and reduce metastatic-associated outcomes in a TNBC stem-like cell model.

Cancer stem cells, resistance, metastatic potential, OXPHOS, mitochondria, chemoprevention

Introduction

Triple-negative breast cancer (TNBC) is an aggressive breast cancer subtype associated with poor clinical outcomes and a high risk of recurrence and metastatic progression [1–3]. Despite advances in systemic therapy, residual tumor cells may survive treatment and contribute to disease relapse and subsequent dissemination. Cancer stem cells (CSCs), also referred to as tumor-initiating, tumor-propagating, or stem-like cancer cells, have been implicated in these processes because of their self-renewal capacity, phenotypic plasticity, and ability to regenerate heterogeneous tumor populations [4, 5]. CSC-like cells may evade treatment through multiple mechanisms, including altered oncogenic signaling, increased expression of ATP-binding cassette transporters, enhanced DNA repair, and resistance to apoptosis [6]. Therapeutic pressure may further select for cellular populations with survival advantages, potentially contributing to residual disease and metastatic progression [7, 8]. Identifying vulnerabilities that persist in these populations is therefore an important objective in the development of strategies to prevent recurrence and metastasis.

Accumulating evidence implicates mitochondrial function and metabolic reprogramming in the maintenance of CSC properties [9–12]. Mitochondria regulate cellular bioenergetics, redox homeostasis, and signaling pathways associated with stemness and differentiation. However, the relative contributions of glycolysis and oxidative phosphorylation (OXPHOS) to CSC maintenance remain context-dependent, and published findings are not entirely consistent [13, 14]. Increased mitochondrial activity and OXPHOS dependence were observed in ovarian [15], small cell lung [16], pancreatic [17], colon [18] and quiescent leukemia CSCs [19]. Glioblastoma CSCs relied on OXPHOS, whereas their

differentiated progeny generated energy primarily through aerobic glycolysis [20]. Data on breast cancer CSCs are contradictory. CSCs in mouse and human tumors have a more glycolytic phenotype compared to non-CSC cells [21], while their dependence on OXPHOS has also been shown [22]. Stem-like populations have been implicated in metastatic dissemination and colonization, raising the possibility that their metabolic dependencies could be targeted to reduce metastatic progression [23–27].

In this study, mammosphere-derived TNBC cells exhibited mitochondrial elongation, increased OXPHOS complex expression, and enhanced respiration. Amoxicillin (AMX) and fosmidomycin sodium salt (FSS) suppressed mammosphere formation and impaired mitochondrial function. In vivo, mammosphere-derived cells were associated with greater lymph-node enlargement and lung nodule burden than parental cells, and AMX reduced both outcomes. AMX pretreatment also delayed tumor establishment. These findings suggest that mitochondrial metabolism may represent a therapeutic vulnerability of TNBC stem-like cells, warranting further investigation as a strategy to address residual disease and metastatic progression.

Methods

Cell culture and generation of chemoresistant cells

Human TNBC cell lines MDA-MB-468 and MDA-MB-231 were purchased from ATCC and authenticated in Ana Janec's lab (UPF, Barcelona). Cells were cultured in antibiotic-free DMEM supplemented with 10% fetal bovine serum (FBS), 1% sodium pyruvate, and 1% L-glutamine at 37°C in 5% CO_2.

Mammosphere culture

CSC-enriched mammospheres were generated by plating single-cell suspensions (10–12 x 10^3 cells/mL) in Poly-HEMA-coated 24-well plates in serum-free stem cell medium containing B27 supplement, insulin (5 µg/mL), EGF (20 ng/mL), and bFGF (10 ng/mL). Primary spheres were collected after 5–7 days, dissociated enzymatically, and re-plated to generate subsequent generations. Third-generation mammospheres were used for all experiments which were performed independently at least twice with 5–6 technical replicates per condition. OXPHOS inhibitors Amoxicillin (AMX) and Fosmidomycin sodium salt (FSS) were added before 3d generation.

Cell viability assay

Cell viability was determined either by the MTT assay or by manual counting wih Trypan Blue inclusion method. Cells were treated with the indicated drugs, incubated with MTT (0.5 mg/mL) for 2 h, and formazan crystals were dissolved in DMSO/ethanol (1:1). Absorbance was measured at 570 nm, and viability was expressed relative to untreated controls.

RT-qPCR

Total RNA was isolated using the RNeasy Mini Kit (Qiagen) and reverse-transcribed using the Maxima First Strand cDNA Synthesis Kit (Thermo Fisher). Quantitative PCR was performed using FastStart Essential DNA Green Master Mix (Roche). Relative gene expression was calculated using the Pfaffl method with ACTB as the reference gene. Primer sequences are provided in Supplementary Table 1.

Protein oxidation analysis

Protein carbonylation was evaluated using the OxyBlot Protein Oxidation Detection Kit (Millipore) according to the manufacturer's instructions. Total protein lysates were derivatized with 2,4-dinitrophenylhydrazine (DNPH), separated by SDS-PAGE, and analyzed by immunoblotting using anti-DNP antibodies. Protocol and original blot are provided in Supplementary Fig. 2.

Seahorse analysis

Mitochondrial respiration was assessed using the Seahorse XFe24 Analyzer (Agilent). Cells (5×10^4/well) were seeded in XF24 plates and analyzed using the Cell Mito Stress Test Kit according to the manufacturer's protocol. Oxygen consumption rates (OCR) were normalized to total protein content determined by BCA assay.

Transmission electron microscopy (TEM)

TEM was performed essentially as described previously [28].

Western blotting

Protein extracts were quantified by BCA assay, separated on 4–20% or 21% SDS-PAGE gels, transferred to nitrocellulose membranes, and probed with antibodies against LC3, p62, p16, BMI1, and β-actin (Supplementary Table 2). Immunoreactive bands were detected using HRP-conjugated secondary antibodies and enhanced chemiluminescence. Original blots are provided in Supplementary Fig. 2.

Plasmid transfection and assessment of mitophagy

Cells were transiently transfected with the pRFP-LC3 plasmid (Addgene) using Lipofectamine 2000 (Thermo Fisher Scientific) according to the manufacturer's protocol. OXPHOS inhibitors were added immediately after transfection, and cells were incubated for an additional 48 h. RFP-LC3 puncta were visualized using a Nikon A1R inverted fluorescence microscope equipped with a ×40 objective (561 nm excitation). At least 25 randomly selected cells per condition were analyzed, and the average number of LC3 puncta per cell was quantified. To evaluate mitophagy, cells were co-stained with 1 μM MitoTracker Green (Thermo Fisher Scientific), and the percentage of LC3 puncta colocalizing with mitochondria was determined using ImageJ software.

Tumor xenograft studies

All animal procedures were approved by Gebze Technical University ethical committte (2024-08 and 2025-03, attached in Supplementary Fig. 4). Female NMRI-nu mice (8 weeks old) were subcutaneously injected with 1 × 10^6 cells mixed with Matrigel. Once tumors reached ~ 100 mm^3, mice were randomized to receive vehicle or the OXPHOS inhibitor Amx (100 mg/kg in drinking water, twice weekly). Tumor volume and body weight were monitored twice weekly. Enlarged ipsilateral inguinal and axillary lymph nodes as well as visible lung nodules were counted after necropsy by visual.

Statistical analysis

All experiments were performed independently at least three times, each with 2–3 technical replicates, unless otherwise indicated. Data are presented as mean ± SEM. Statistical analyses were performed using GraphPad Prism 8.0.1 (GraphPad Software). Differences between groups were analyzed by two-way ANOVA followed by an appropriate multiple-comparison post hoc test. A value of $P < 0.05$ was considered statistically significant.

Results

Given the established role of mitochondria in maintaining stemness [29, 30], we investigated metabolic plasticity in CSC-like cells using third-generation mammospheres derived from the TNBC cell lines MDA-MB-468 and MDA-MB-231. Mammosphere formation provides a functional approach to enriching stem-like cancer cell populations and may help identify phenotypes associated with tumor initiation and metastatic potential, although it does not directly establish metastatic capacity. TNBC cell lines were selected because stemness-associated markers are expressed at substantially higher levels in TNBC than in other breast cancer subtypes, as demonstrated by our bioinformatic analyses (Supplementary Fig. 1). The mammospheres exhibited increased expression of stemness markers (Fig. 1A, Supplementary Fig. 2A) greater resistance to cisplatin than their parental counterparts (Fig. 1B), supporting their relevance as a model of treatment-resistant, CSC-like populations that may contribute to residual disease and subsequent metastatic progression.

Because mitochondrial characteristics may influence the survival and adaptability of tumor cells during progression [31], we examined mitochondrial morphology and function in these populations. Electron microscopy revealed that, despite comparable mitochondrial numbers, mammosphere-derived cells contained more elongated mitochondria with denser cristae and a larger mitochondrial area than parental cells (Fig. 1C,D). Furthermore, expression of mitochondrial respiratory-chain complex proteins increased across successive mammosphere generations (Fig. 1E, Supplementary Fig. 2C). Consistent with these change, Seahorse analysis demonstrated elevated oxygen consumption rate (OCR) and maximal respiratory capacity in mammospheres (Fig. 1F,G). These findings indicate that TNBC mammosphere-derived CSC-like cells exhibit enhanced mitochondrial activity alongside stemness-associated and chemoresistant phenotypes. Such metabolic features may support the persistence of tumor-initiating populations and warrant further investigation into whether OXPHOS dependence contributes to their potential role in metastatic progression [32].

Mammosphere-forming capacity is a functional indicator of CSC-like activity and has been associated with tumor initiation, chemoresistance, metastatic potential, and poor prognosis [33, 34]. Our recent findings further link cancer stemness and treatment resistance to metastatic potential and identify OXPHOS as a potential therapeutic target [35, 36]. Consistent with this rationale, our unpublished observations indicate that chemoresistant cells form mammospheres more efficiently than parental cells (Supplementary Fig. 3). Here, several prescreened OXPHOS-targeting agents significantly reduced mammosphere formation (Fig. 2A,B, Supplementary Fig. 3) and preferentially suppressed mitochondrial respiration and maximal respiratory capacity in mammospheres compared with parental cells (Fig. 2C-F). These findings suggest that mitochondrial metabolism may support CSC-like properties associated with tumor persistence and metastatic progression.

Repurposed antimicrobials have previously been proposed as potential OXPHOS-targeting agents in CSCs [37, 38] and other studies have demonstrated the feasibility of using antimicrobials to inhibit leukemia in vivo [39, 40]. However, the mechanisms underlying their effects in eukaryotic cells remain incompletely understood. Building on our previous work linking OXPHOS inhibition to autophagy [41–43], we investigated mitochondrial quality control following treatment with tolerable OXPHOS inhibitors AMX and FSS. Both agents induced lipidated LC3 in CSC-like cells (Fig. 3A,B, Supplementary Fig. 2B), while immunofluorescence revealed colocalization of LC3 puncta with mitochondrial signals, consistent with increased mitophagy-associated activity (Fig. 3C,D). OXPHOS inhibition also increased protein carbonylation, indicating oxidative protein damage (Fig. 3E, Supplementary Fig. 2C), consistent with our previous findings linking reactive oxygen species to mitophagy [44]. Together, these results suggest that disrupting mitochondrial function and redox homeostasis may impair mammosphere-forming CSC-like populations.

Finally, immunocompromised mice were xenografted subcutaneously with parental or mammosphere-derived CSC-like cells (1×10^6 cells per flank). After tumors had developed for 14 days, animals were randomized to receive oral AMX in PBS or PBS alone for seven weeks (Fig. 4A). AMX significantly reduced tumor growth and final tumor volume in the CSC-like cell-derived group, while having a limited effect on parental cell-derived tumors (Fig. 4B,C, Supplementary Fig. 4–10). Importantly, mice injected with mammosphere-derived cells exhibited approximately 2.5-fold more enlarged ipsilateral inguinal and axillary lymph nodes (3–5 mm in diameter) and twice as many visible lung nodules (~ 1 mm) as mice injected with parental cells (Fig. 4D,E). AMX treatment significantly reduced both the number of enlarged lymph nodes and the number of visible lung nodules in the mammosphere-derived group, with no comparable effect in mice bearing parental cell-derived tumors. These findings link the CSC-like phenotype with increased observed metastatic-associated outcomes in vivo and suggest that targeting mitochondrial metabolism may preferentially affect tumor-initiating populations associated with these outcomes. In a complementary experiment, mice received AMX in drinking water for approximately two weeks before subcutaneous implantation of parental or mammosphere-derived cells (Fig. 4F). This pretreatment delayed tumor growth, with a statistically significant effect in the mammosphere-derived group but not in the parental-cell group (Fig. 4G, Supplementary Fig. 4–10). Together, these findings suggest that AMX preferentially impairs tumor establishment by CSC-like TNBC populations and reduces

associated lymph-node enlargement and lung nodule burden, supporting further investigation of mitochondrial targeting as a strategy to limit CSC-associated metastatic progression.

Discussion

Our findings support mitochondrial oxidative phosphorylation (OXPHOS) as a potential therapeutic vulnerability of cancer stem-like cells (CSCs), which may contribute to tumor recurrence, treatment resistance, and metastatic progression. Therapy-resistant populations may emerge through selection of pre-existing, slowly proliferating CSCs or drug-tolerant persister cells, or through dynamic metabolic reprogramming toward OXPHOS, as reported in leukemia [39], colorectal cancer [45], prostate cancer [46], and non-small cell lung cancer [47, 48]. Experimental conditions also influence metabolic phenotypes: high-glucose culture media can favor glycolysis [49], while standard antibiotics may alter mitochondrial OXPHOS [50]. In addition, fatty acid oxidation and other lipid metabolic pathways can support CSC self-renewal, redox homeostasis, and chemoresistance [51–55], highlighting the metabolic plasticity that may facilitate tumor progression and adaptation to treatment.

In our TNBC models, mammosphere-derived CSC-like cells exhibited enhanced mitochondrial activity and tumor-initiating properties. Pharmacological intervention targeting mitochondrial metabolism suppressed mammosphere formation and respiration and increased oxidative stress and protein damage, with associated changes in mitophagy. In vivo, mammosphere-derived cells were associated with greater lymph-node enlargement and lung nodule burden than parental cells, while amoxicillin treatment reduced both outcomes in the mammosphere-derived group. Amoxicillin pretreatment also delayed subsequent tumor establishment. Although histological confirmation is required to establish the tumor origin of the lymph-node and lung findings, these observations support further investigation of mitochondrial metabolism as a vulnerability of CSC-like populations associated with metastatic disease.

These findings provide a rationale for evaluating OXPHOS-targeting strategies to limit tumor establishment and potentially reduce metastatic progression and residual disease. Future studies using patient-derived systems and single-cell metabolic analyses are needed to establish whether mitochondrial dependence can serve as a predictive biomarker and whether selective targeting of OXPHOS can improve the efficacy of conventional anticancer therapies.

Declarations

Contributions

CU: Validation, Methodology, Formal analysis. EA: Validation, Methodology, Formal analysis. MG: Validation, Methodology, Formal analysis. EK: Formal analysis. CT and ZU: Methodology, Formal analysis. EA: Validation, Methodology. AL: Writing – original draft, review & editing, Methodology, Formal analysis, Conceptualization, Supervision, Funding acquisition.

Availability of data and materials

All data included in this study are available upon request by contact with the corresponding author.

Funding

A.L. and lab members were supported by the TUBITAK 2232A program (Project 121C096) and TUBITAK 1001 grant (Project 124Z377) without expences for publication costs.

Acknowledgements

We thank Gebze Technique University animal facility staff for their support.

Competing interests

The authors declare no competing interests.

Ethical Approvals

All experimental procedures involving animals were performed in accordance with the National Institutes of Health Guide for the Care and Use of Laboratory Animals and approved by Gebze Technical University ethical committte (2024-08 and 2025-03, attached in Supplementary Fig. 4). Arrival 2.0 is completed.

References

1. Lambert AW, Pattabiraman DR, Weinberg RA (2017) Emerg Biol Principles Metastasis Cell 168:670–691. https://doi.org/10.1016/j.cell.2016.11.037
2. Rivera E, Gomez H (2010) Chemotherapy resistance in metastatic breast cancer: the evolving role of ixabepilone. Breast Cancer Res 12 Suppl 2S2. https://doi.org/10.1186/bcr2573
3. Bianchini G, Balko JM, Mayer IA, Sanders ME, Gianni L (2016) Triple-negative breast cancer: challenges and opportunities of a heterogeneous disease. Nat Rev Clin Oncol 13:674–690. https://doi.org/10.1038/nrclinonc.2016.66
4. Bergers G, Fendt S-M (2021) The metabolism of cancer cells during metastasis. Nat Rev Cancer 21:162–180. https://doi.org/10.1038/s41568-020-00320-2
5. Pérez-González A, Bévant K, Blanpain C (2023) Cancer cell plasticity during tumor progression, metastasis and response to therapy. Nat Cancer 4:1063–1082. https://doi.org/10.1038/s43018-023-00595-y
6. Abad E, Graifer D, Lyakhovich A (2020) DNA damage response and resistance of cancer stem cells. Cancer Lett 474:106–117. https://doi.org/10.1016/j.canlet.2020.01.008
7. Soteriou D, Fuchs Y (2018) A matter of life and death: stem cell survival in tissue regeneration and tumour formation. Nat Rev Cancer 18:187–201. https://doi.org/10.1038/nrc.2017.122
8. Zhao J (2016) Cancer stem cells and chemoresistance: The smartest survives the raid. Pharmacol Ther 160:145–158. https://doi.org/10.1016/j.pharmthera.2016.02.008

9. Faubert B, Solmonson A, DeBerardinis RJ (2020) Metabolic reprogramming and cancer progression. Science 368. https://doi.org/10.1126/science.aaw5473
10. Zheng X-X, Chen J-J, Sun Y-B, Chen T-Q, Wang J, Yu S-C (2023) Mitochondria in cancer stem cells: Achilles heel or hard armor. Trends Cell Biol 33:708–727. https://doi.org/10.1016/j.tcb.2023.03.009
11. Mauro-Lizcano M, Di Pisa F, Larrea Murillo L, Sugden CJ, Sotgia F, Lisanti MP (2024) High mitochondrial DNA content is a key determinant of stemness, proliferation, cell migration, and cancer metastasis in vivo. Cell Death Dis 15:745. https://doi.org/10.1038/s41419-024-07103-9
12. Chen C-T, Hsu S-H, Wei Y-H (2012) Mitochondrial bioenergetic function and metabolic plasticity in stem cell differentiation and cellular reprogramming. Biochim Biophys Acta 1820:571–576. https://doi.org/10.1016/j.bbagen.2011.09.013
13. Peiris-Pagès M, Martinez-Outschoorn UE, Pestell RG, Sotgia F, Lisanti MP (2016) Cancer stem cell metabolism. Breast Cancer Res 18:55. https://doi.org/10.1186/s13058-016-0712-6
14. Akkuş E, Lyakhovich A (2025) (2025) Targeting the bioenergetics of a resistant tumor: clinical insights into OXPHOS inhibition for cancer therapy, Redox Exp. Med. https://doi.org/10.1530/REM-25-0003
15. Sato M, Kawana K, Adachi K, Fujimoto A, Yoshida M, Nakamura H, Nishida H, Inoue T, Taguchi A, Takahashi J, Eguchi S, Yamashita A, Tomio K, Wada-Hiraike O, Oda K, Nagamatsu T, Osuga Y, Fujii T (2016) Spheroid cancer stem cells display reprogrammed metabolism and obtain energy by actively running the tricarboxylic acid (TCA) cycle. Oncotarget 7:33297–33305. https://doi.org/10.18632/oncotarget.8947
16. Gao C, Shen Y, Jin F, Miao Y, Qiu X (2016) Cancer Stem Cells in Small Cell Lung Cancer Cell Line H446: Higher Dependency on Oxidative Phosphorylation and Mitochondrial Substrate-Level Phosphorylation than Non-Stem Cancer Cells. PLoS ONE 11:e0154576. https://doi.org/10.1371/journal.pone.0154576
17. Sancho P, Burgos-Ramos E, Tavera A, Bou Kheir T, Jagust P, Schoenhals M, Barneda D, Sellers K, Campos-Olivas R, Graña O, Viera CR, Yuneva M, Sainz B, Heeschen C (2015) MYC/PGC-1α Balance Determines the Metabolic Phenotype and Plasticity of Pancreatic Cancer Stem Cells. Cell Metab 22:590–605. https://doi.org/10.1016/j.cmet.2015.08.015
18. Denise C, Paoli P, Calvani M, Taddei ML, Giannoni E, Kopetz S, Kazmi SMA, Pia MM, Pettazzoni P, Sacco E, Caselli A, Vanoni M, Landriscina M, Cirri P, Chiarugi P (2015) 5-fluorouracil resistant colon cancer cells are addicted to OXPHOS to survive and enhance stem-like traits. Oncotarget 6:41706–41721. https://doi.org/10.18632/oncotarget.5991
19. Lagadinou ED, Sach A, Callahan K, Rossi RM, Neering SJ, Minhajuddin M, Ashton JM, Pei S, Grose V, O'Dwyer KM, Liesveld JL, Brookes PS, Becker MW, Jordan CT (2013) BCL-2 inhibition targets oxidative phosphorylation and selectively eradicates quiescent human leukemia stem cells. Cell Stem Cell 12:329–341. https://doi.org/10.1016/j.stem.2012.12.013
20. Vlashi E, Lagadec C, Vergnes L, Matsutani T, Masui K, Poulou M, Popescu R, Della Donna L, Evers P, Dekmezian C, Reue K, Christofk H, Mischel PS, Pajonk F (2011) Metabolic state of glioma stem cells

and nontumorigenic cells., Proc. Natl. Acad. Sci. U. S. A. 108 16062–7. https://doi.org/10.1073/pnas.1106704108

21. Feng W, Gentles A, Nair RV, Huang M, Lin Y, Lee CY, Cai S, Scheeren FA, Kuo AH, Diehn M (2014) Targeting unique metabolic properties of breast tumor initiating cells. Stem Cells 32:1734–1745. https://doi.org/10.1002/stem.1662
22. Vlashi E, Lagadec C, Vergnes L, Reue K, Frohnen P, Chan M, Alhiyari Y, Dratver MB, Pajonk F (2014) Metabolic differences in breast cancer stem cells and differentiated progeny. Breast Cancer Res Treat 146:525–534. https://doi.org/10.1007/s10549-014-3051-2
23. Magee JA, Piskounova E, Morrison SJ (2012) Cancer stem cells: impact, heterogeneity, and uncertainty. Cancer Cell 21:283–296. https://doi.org/10.1016/j.ccr.2012.03.003
24. Pattabiraman DR, Weinberg RA (2014) Tackling the cancer stem cells - what challenges do they pose? Nat Rev Drug Discov 13:497–512. https://doi.org/10.1038/nrd4253
25. Medema JP (2013) Cancer stem cells: the challenges ahead. Nat Cell Biol 15:338–344. https://doi.org/10.1038/ncb2717
26. Liu Y, Nenutil R, Appleyard MV, Murray K, Boylan M, Thompson AM, Coates PJ (2014) Lack of correlation of stem cell markers in breast cancer stem cells. Br J Cancer 110:2063–2071. https://doi.org/10.1038/bjc.2014.105
27. Karp I, Lyakhovich A (2022) Targeting cancer stem cells with antibiotics inducing mitochondrial dysfunction as an alternative anticancer therapy. Biochem Pharmacol 198:114966. https://doi.org/10.1016/j.bcp.2022.114966
28. Kumari U, Ya Jun W, Huat Bay B, Lyakhovich A (2014) Evidence of mitochondrial dysfunction and impaired ROS detoxifying machinery in Fanconi anemia cells. Oncogene 33:165–172. https://doi.org/10.1038/onc.2012.583
29. Cuyàs E, Verdura S, Folguera-Blasco N, Bastidas-Velez C, Martin ÁG, Alarcón T, Menendez JA (2018) Mitostemness Cell Cycle 17:918–926. https://doi.org/10.1080/15384101.2018.1467679
30. Shibue T, Weinberg RA (2017) EMT, CSCs, and drug resistance: the mechanistic link and clinical implications. Nat Rev Clin Oncol 14:611–629. https://doi.org/10.1038/nrclinonc.2017.44
31. Jadav N, Velamoor S, Huang D, Cassin L, Hazelton N, Eruera A-R, Burga LN, Bostina M (2023) Beyond the surface: Investigation of tumorsphere morphology using volume electron microscopy. J Struct Biol 215:108035. https://doi.org/10.1016/j.jsb.2023.108035
32. Zheng J (2012) Energy metabolism of cancer: Glycolysis versus oxidative phosphorylation (Review). Oncol Lett 4:1151–1157. https://doi.org/10.3892/ol.2012.928
33. Eyre R, Alférez DG, Spence K, Kamal M, Shaw FL, Simões BM, Santiago-Gómez A, Sarmiento-Castro A, Bramley M, Absar M, Saad Z, Chatterjee S, Kirwan C, Gandhi A, Armstrong AC, Wardley AM, O'Brien CS, Farnie G, Howell SJ, Clarke RB (2016) Patient-derived Mammosphere and Xenograft Tumour Initiation Correlates with Progression to Metastasis. J Mammary Gland Biol Neoplasia 21:99–109. https://doi.org/10.1007/s10911-016-9361-8

34. Paholak HJ, Stevers NO, Chen H, Burnett JP, He M, Korkaya H, McDermott SP, Deol Y, Clouthier SG, Luther T, Li Q, Wicha MS, Sun D (2016) Elimination of epithelial-like and mesenchymal-like breast cancer stem cells to inhibit metastasis following nanoparticle-mediated photothermal therapy. Biomaterials 104:145–157. https://doi.org/10.1016/j.biomaterials.2016.06.045
35. Abad E, García-Mayea Y, Mir C, Sebastian D, Zorzano A, Potesil D, Zdrahal Z, Lyakhovich A, Lleonart ME (2019) Common Metabolic Pathways Implicated in Resistance to Chemotherapy Point to a Key Mitochondrial Role in Breast Cancer., Mol. Cell Proteom 18:231–244. https://doi.org/10.1074/mcp.RA118.001102
36. Uslu C, Kapan E, Lyakhovich A (2025) OXPHOS inhibition overcomes chemoresistance in triple negative breast cancer. Redox Biol 83:103637. https://doi.org/10.1016/j.redox.2025.103637
37. Fiorillo M, Lamb R, Tanowitz HB, Cappello AR, Martinez-Outschoorn UE, Sotgia F, Lisanti MP (2016) Bedaquiline, an FDA-approved antibiotic, inhibits mitochondrial function and potently blocks the proliferative expansion of stem-like cancer cells (CSCs). Aging (Albany NY) 8:1593–1607. https://doi.org/10.18632/aging.100983
38. Fiorillo M, Tóth F, Sotgia F, Lisanti MP (2019) Doxycycline, Azithromycin and Vitamin C (DAV): A potent combination therapy for targeting mitochondria and eradicating cancer stem cells (CSCs)., Aging (Albany. NY). 11:2202–2216. https://doi.org/10.18632/aging.101905
39. Kuntz EM, Baquero P, Michie AM, Dunn K, Tardito S, Holyoake TL, Helgason GV, Gottlieb E (2017) Targeting mitochondrial oxidative phosphorylation eradicates therapy-resistant chronic myeloid leukemia stem cells. Nat Med 23:1234–1240. https://doi.org/10.1038/nm.4399
40. Himonas E, de Beauchamp L, Zerbst D, Desmares-Romain E, Sarnello D, Kalkman ER, Rattigan KM, James D, Shokry E, Copland M, Griessinger E, Récher C, De Mas V, Vergez F, Sumpton D, Schimmer AD, Minden MD, Gottlieb E, Shanks E, Sarry J-E, Helgason GV (2026) A metabolism-specific drug-repurposing screen reveals itraconazole as a potent OXPHOS inhibitor in acute myeloid leukemia. Blood 147:2431–2447. https://doi.org/10.1182/blood.2024027853
41. Esner M, Graifer D, Lleonart ME, Lyakhovich A (2017) Targeting cancer cells through antibiotics-induced mitochondrial dysfunction requires autophagy inhibition. Cancer Lett 384:60–69. https://doi.org/10.1016/j.canlet.2016.09.023
42. Lu Z, Xu N, He B, Pan C, Lan Y, Zhou H, Liu X (2017) Inhibition of autophagy enhances the selective anti-cancer activity of tigecycline to overcome drug resistance in the treatment of chronic myeloid leukemia. J Exp Clin Cancer Res 36:43. https://doi.org/10.1186/s13046-017-0512-6
43. Lyakhovich A, Graifer D (2015) Mitochondria-Mediated Oxidative Stress: Old Target for New Drugs. Curr Med Chem 22:3040–3053. https://doi.org/10.2174/0929867322666150729114036
44. Rappeport JR (1985) Reasonable medical certainty. Bull Am Acad Psychiatry Law 13:5–15
45. Vellinga TT, Borovski T, de Boer VCJ, Fatrai S, van Schelven S, Trumpi K, Verheem A, Snoeren N, Emmink BL, Koster J, Rinkes IHMB, Kranenburg O (2015) SIRT1/PGC1α-Dependent Increase in Oxidative Phosphorylation Supports Chemotherapy Resistance of Colon Cancer., Clin. Cancer Res 21:2870–2879. https://doi.org/10.1158/1078-0432.CCR-14-2290

46. Ippolito L, Marini A, Cavallini L, Morandi A, Pietrovito L, Pintus G, Giannoni E, Schrader T, Puhr M, Chiarugi P, Taddei ML (2016) Metabolic shift toward oxidative phosphorylation in docetaxel resistant prostate cancer cells. Oncotarget 7:61890–61904. https://doi.org/10.18632/oncotarget.11301
47. Lee S, Lee J-S, Seo J, Lee S-H, Kang JH, Song J, Kim S-Y (2018) Targeting Mitochondrial Oxidative Phosphorylation Abrogated Irinotecan Resistance in NSCLC. Sci Rep 8:15707. https://doi.org/10.1038/s41598-018-33667-6
48. Chen D, Barsoumian HB, Fischer G, Yang L, Verma V, Younes AI, Hu Y, Masropour F, Klein K, Vellano C, Marszalek J, Davies M, Cortez MA, Welsh J (2020) Combination treatment with radiotherapy and a novel oxidative phosphorylation inhibitor overcomes PD-1 resistance and enhances antitumor immunity. J Immunother Cancer 8. https://doi.org/10.1136/jitc-2019-000289
49. Suganuma K, Miwa H, Imai N, Shikami M, Gotou M, Goto M, Mizuno S, Takahashi M, Yamamoto H, Hiramatsu A, Wakabayashi M, Watarai M, Hanamura I, Imamura A, Mihara H, Nitta M (2010) Energy metabolism of leukemia cells: glycolysis versus oxidative phosphorylation. Leuk Lymphoma 51:2112–2119. https://doi.org/10.3109/10428194.2010.512966
50. Fadda H, Khan RH, Shqair Y, Uslu C, Panov AV, Lyakhovich A (2025) Antibacterials exert toxic effects on aquatic organisms by inhibiting respiration, inducing oxidative stress, mitochondrial dysfunction and autophagy. Aquat Toxicol 280:107284. https://doi.org/10.1016/j.aquatox.2025.107284
51. Park JH, Vithayathil S, Kumar S, Sung P-L, Dobrolecki LE, Putluri V, Bhat VB, Bhowmik SK, Gupta V, Arora K, Wu D, Tsouko E, Zhang Y, Maity S, Donti TR, Graham BH, Frigo DE, Coarfa C, Yotnda P, Putluri N, Sreekumar A, Lewis MT, Creighton CJ, Wong L-JC, Kaipparettu BA (2016) Fatty Acid Oxidation-Driven Src Links Mitochondrial Energy Reprogramming and Oncogenic Properties in Triple-Negative Breast Cancer. Cell Rep 14:2154–2165. https://doi.org/10.1016/j.celrep.2016.02.004
52. Ye H, Adane B, Khan N, Sullivan T, Minhajuddin M, Gasparetto M, Stevens B, Pei S, Balys M, Ashton JM, Klemm DJ, Woolthuis CM, Stranahan AW, Park CY, Jordan CT (2016) Cell Stem Cell 19:23–37. Leukemic Stem Cells Evade Chemotherapy by Metabolic Adaptation to an Adipose Tissue Nichehttps://doi.org/10.1016/j.stem.2016.06.001
53. Pascual G, Avgustinova A, Mejetta S, Martín M, Castellanos A, Attolini CS-O, Berenguer A, Prats N, Toll A, Hueto JA, Bescós C, Di Croce L, Benitah SA (2017) Targeting metastasis-initiating cells through the fatty acid receptor CD36. Nature 541:41–45. https://doi.org/10.1038/nature20791
54. Mancini R, Noto A, Pisanu ME, De Vitis C, Maugeri-Saccà M, Ciliberto G (2018) Metabolic features of cancer stem cells: the emerging role of lipid metabolism. Oncogene 37:2367–2378. https://doi.org/10.1038/s41388-018-0141-3
55. Daniel Y, Lelou E, Aninat C, Corlu A, Cabillic F (2021) Interplay between Metabolism Reprogramming and Epithelial-to-Mesenchymal Transition in Cancer Stem Cells. Cancers (Basel) 13. https://doi.org/10.3390/cancers13081973

Figures

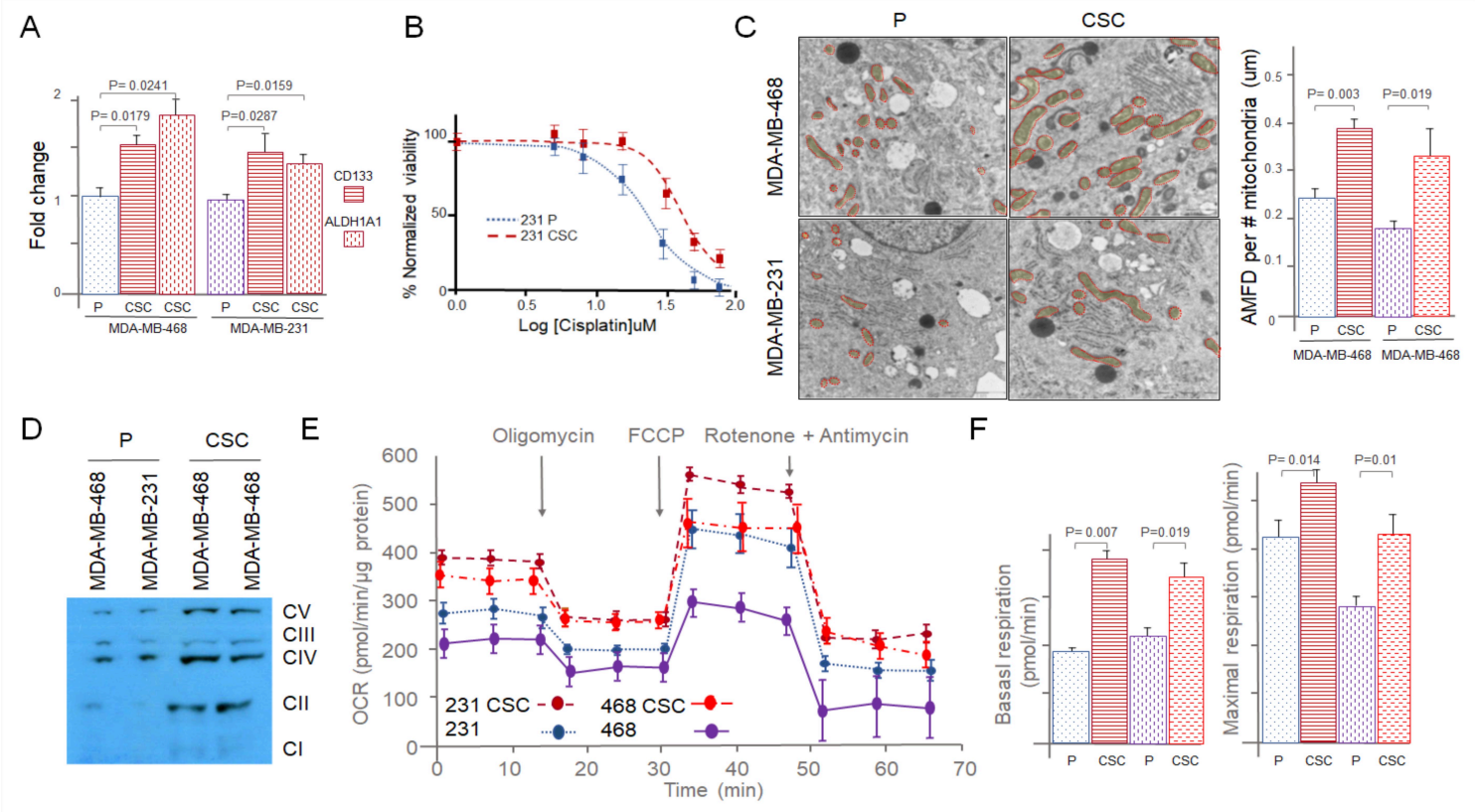


Figure 1

Acquisition of the cancer stem cell phenotype is associated with enhanced mitochondrial OXPHOS activity in TNBC cells. A RT-qPCR analysis of the indicated stemness-related genes in parental (P) MDA-MB-468 and MDA-MB-231 TNBC cells and their corresponding mammospheres (CSC). Five replicates are shown. **B** Cell survivability assay in the presence of cisplatin. **C** Representative transmission electron micrographs of parental (P) and CSC-like cells. Scale bars, 1 µm. Mitochondria are highlighted in orange. **D**Mitochondrial size was quantified by measuring the Feret's diameter of approximately 100 mitochondria per sample using QuPath software. Mean mitochondrial Feret's diameter is presented as bar graphs. Statistical significance was determined by one-way ANOVA, n>30. **E** Representative immunoblots showing the expression of mitochondrial OXPHOS complex subunits in parental (P) cells and CSC-like mammospheres. **F** Mitochondrial respiration was assessed using the Seahorse XFe24 Analyzer (Agilent Technologies). **G** Oxygen consumption rate was measured under basal conditions and following sequential injection of oligomycin (ATP synthase inhibitor) and the mitochondrial uncoupler carbonyl cyanide-4-(trifluoromethoxy)phenylhydrazone (FCCP) to determine maximal respiratory capacity. Data are presented as mean ± SD (n ≥ 3). To see this illustration in color, the reader is referred to the online version of this article.

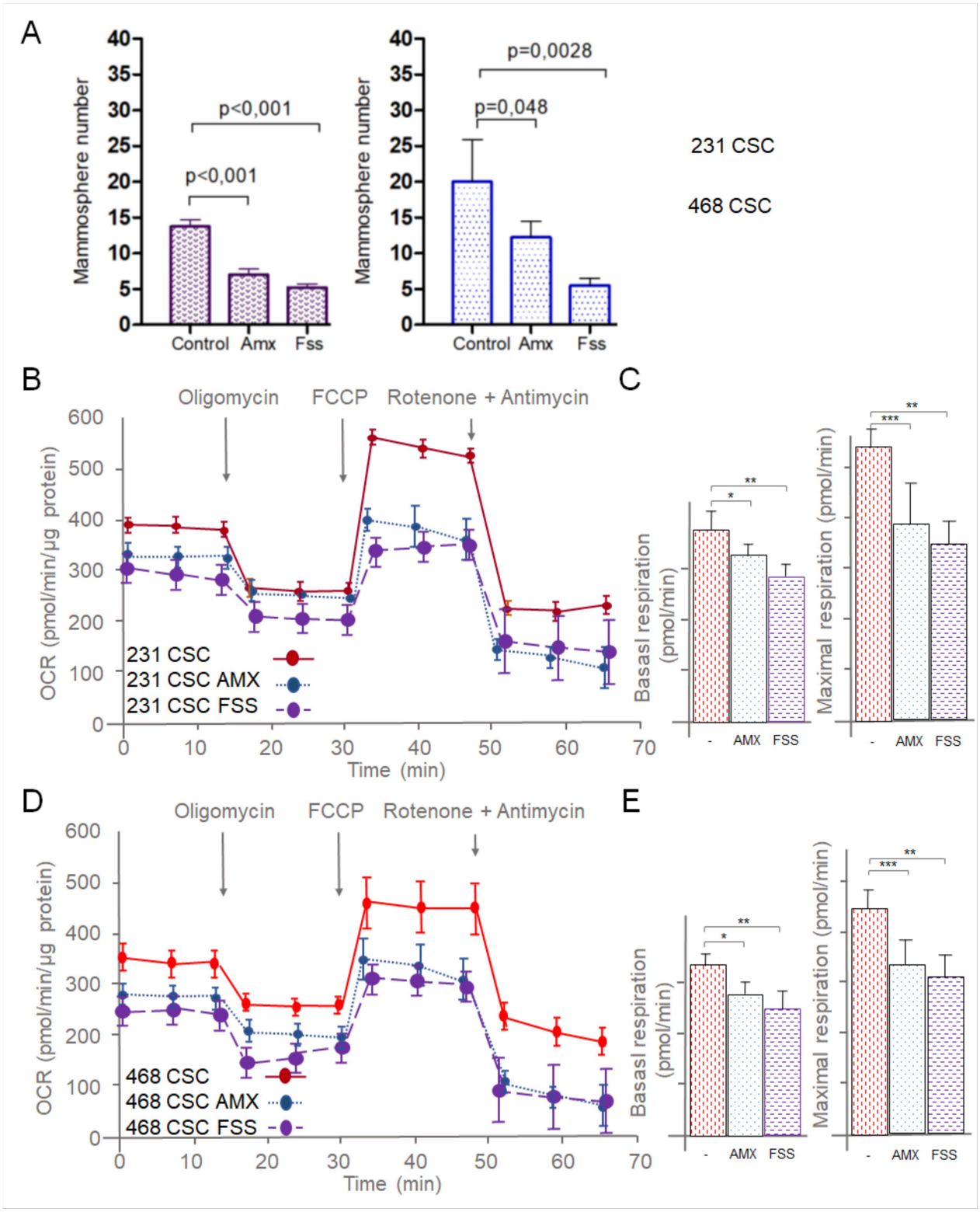


Figure 2

OXPHOS inhibitors suppress mammosphere formation and mitochondrial respiration in TNBC cells with metastasis-associated CSC-like properties. A Mammosphere formation assay in MDA-MB-468 and MDA-MB-231 TNBC cells pretreated with the OXPHOS inhibitors AMX or FSS for 3 days, or with vehicle (DMSO, control), followed by culture under mammosphere-forming conditions for 10 days. Representative images and quantification of mammosphere formation are provided in Supplementary

Fig. S3. Mitochondrial respiration was assessed in parental and mammosphere-derived MDA-MB-231 **B** and MDA-MB-468 **C** TNBC cells following treatment with the indicated OXPHOS inhibitors using the Seahorse XFe24 Analyzer (Agilent Technologies). **D,E** Oxygen consumption rate was measured under basal conditions and following sequential injection of oligomycin (ATP synthase inhibitor) and the mitochondrial uncoupler carbonyl cyanide-4-(trifluoromethoxy)phenylhydrazone (FCCP) to determine maximal respiratory capacity. Data are presented as mean ± SD (n ≥ 3). Statistical significance was determined by two-way ANOVA. *P < 0.025, **P < 0.05, and ***P < 0.05 compared with the corresponding untreated control. To see this illustration in color, the reader is referred to the online version of this article.

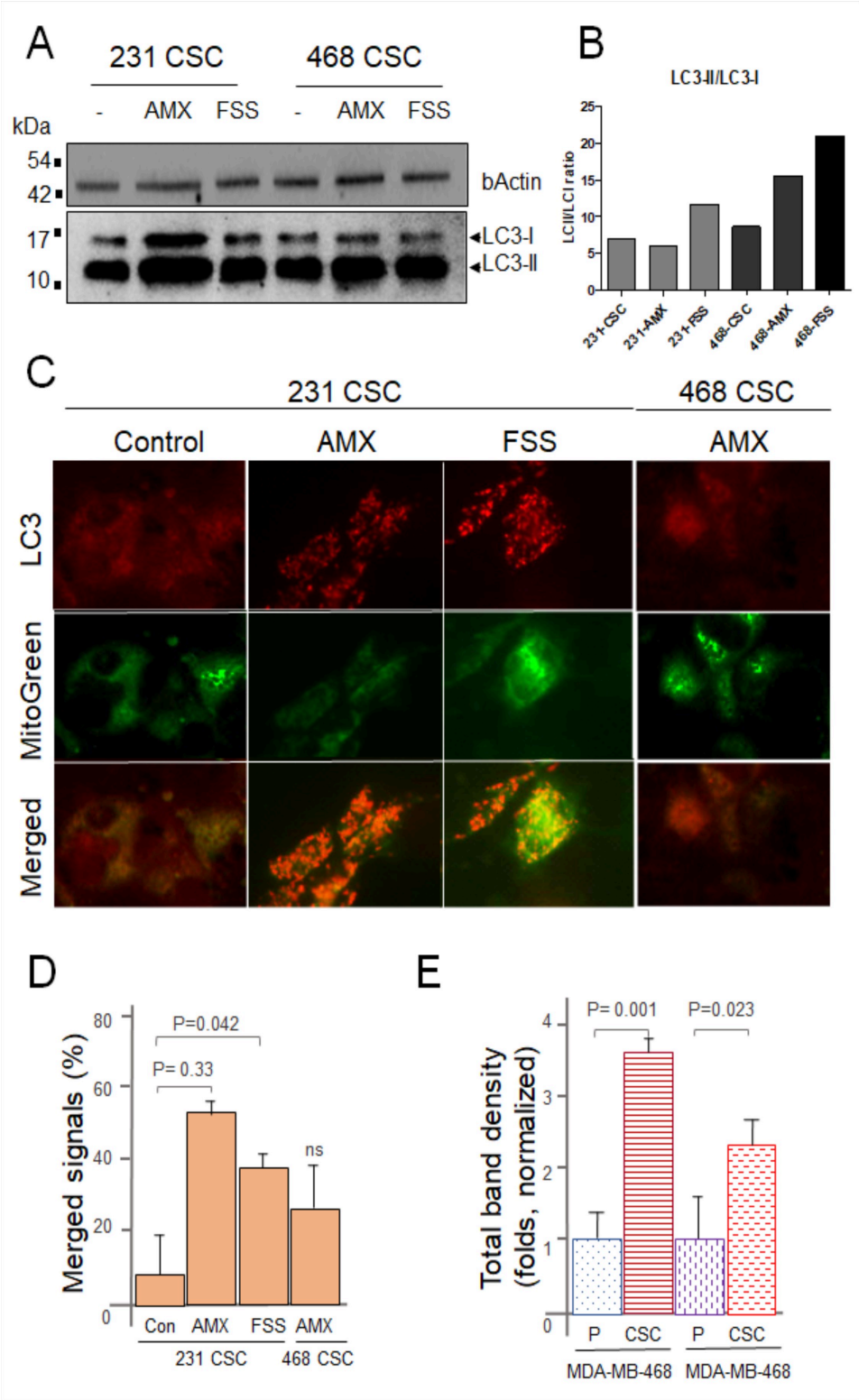


Figure 3

OXPHOS inhibitors induce oxidative stress and mitophagy in CSCs. A Results of Western blot for the autophagy markers LC3-II and p62 demonstrate increased lipidated LC3-II forms in CSC-like mammospheres. Below are shown % of LC3-II lipidated vs nonlipidated signals normalized to loading control. **B** Mammosphers from MDA-MB-468 and MDA-MB-231 cells were transfected with 1 μg of LC3-II-RFP pDNA in 6-well plates and after 2 days were treated with corresponding OXPHOS inhibitors for 1

day. After co-staining with MitoTracker Green reagent, images were taken at 40× magnification and **C** results of merged red and green channels were calculated as the percentage of mitophagic events per cell (n> 25). **D** Oxidative modification of proteins was measured by OxyBlot analyses. TDNP-derivatized cell lysates were analysed for the presence of oxidized protein and average density signals were plotted on the bar diagram after normalization to beta-actin. To see this illustration in color, the reader is referred to the online version of this article.

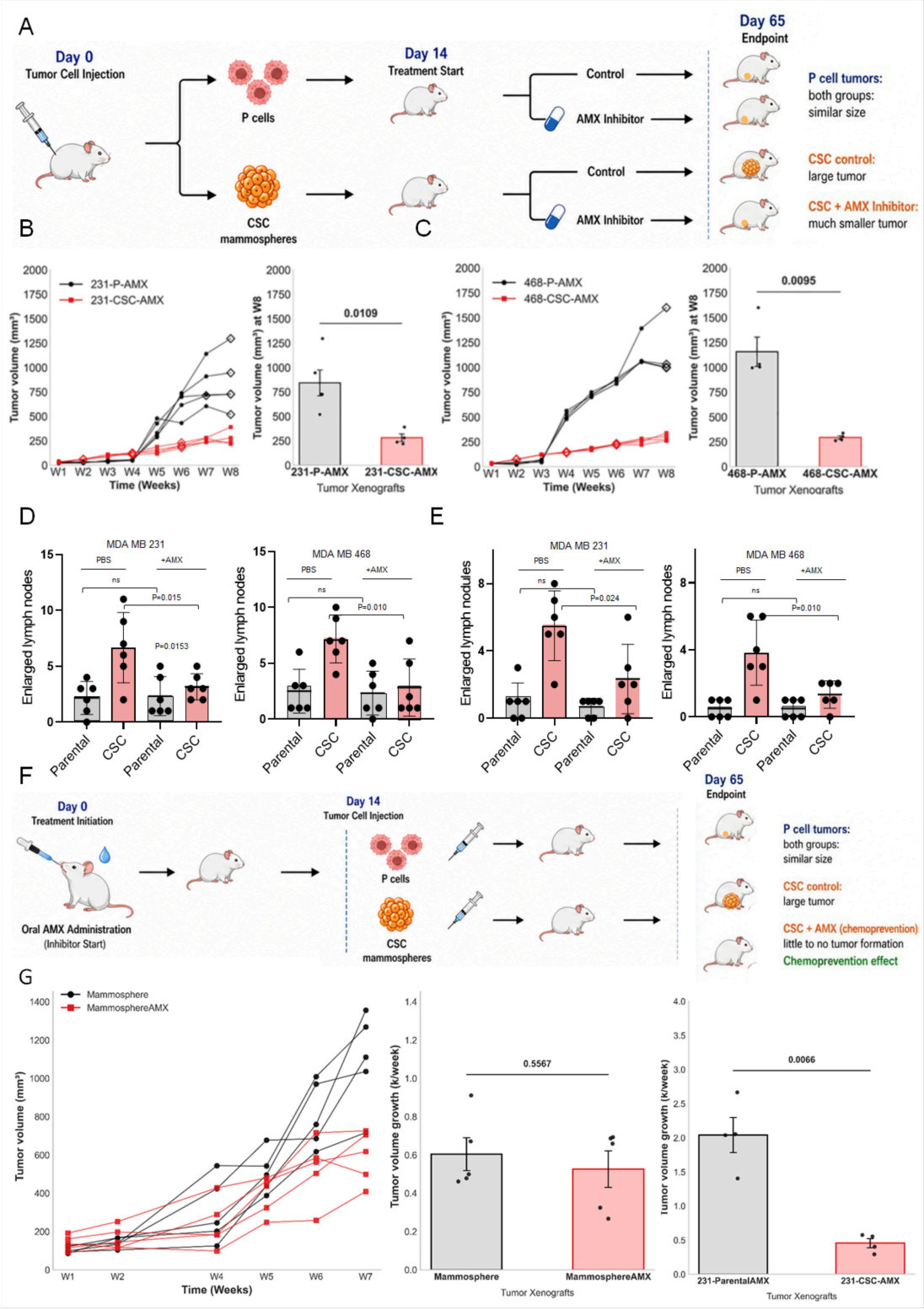


Figure 4

OXPHOS inhibition suppresses CSC-like tumor growth, reduces metastatic lesions, and delays tumor initiation in TNBC xenograft models. A Schematic overview of the therapeutic treatment protocol. **B**MDA-MB-231 and **C** MDA-MB-468 parental TNBC cells (P) and CSC-like mammospheres (1 × 10^6 cells) were mixed 1:1 with Matrigel and injected subcutaneously into opposite flanks of NMRI-nu mice. Once tumors reached approximately 100 mm^3, mice were randomized to receive either the OXPHOS inhibitor AMX (100 mg/kg) or vehicle (PBS) in the drinking water twice weekly. Tumor growth was monitored weekly by caliper measurements, and tumor volume was calculated as [length x width x height (mm)]/2). The graphs show tumor volumes at week 8. **D** Numbers of enlarged ipsilateral inguinal and **E**axillary lymph nodes and visible lung nodules. Unpaired T-test with Welch' correction. **F** Schematic overview of the chemoprevention protocol. NMRI-nu mice were pretreated with either AMX (100 mg/kg) or vehicle (PBS) in the drinking water for 2 weeks before subcutaneous injection of parental TNBC cells or CSC-like mammospheres (1 × 10^6 cells mixed 1:1 with Matrigel). Tumor growth was monitored weekly, and tumor volumes were calculated as [length x width x height (mm)]/2). **G** Tumor volumes at week 7 and tumor growth rates are shown. All original calculations are provided in Supplementary Fig. 4-10. To see this illustration in color, the reader is referred to the online version of this article.

Supplementary Files

This is a list of supplementary files associated with this preprint. Click to download.

- Supplementarymaterial.pdf
- ARRIVE2.0.pdf
- GraphicalAbstract.jpg
- GraphicalAbstract.jpg